

Single-Molecule Magnetic Behavior in a Neutral Terbium(III) Complex of a Picolinate-Based Nitronyl Nitroxide Free Radical

Eugenio Coronado,[†] Carlos Giménez-Saiz,[†] Alejandro Recuenco,[†] Ana Tarazón,[†] Francisco M. Romero,^{*,†} Agustín Camón,[‡] and Fernando Luis[‡][†]Instituto de Ciencia Molecular, Universitat de València, Calle Catedrático José Beltrán 2, 46980 Paterna, Spain[‡]Instituto de Ciencia de Materiales de Aragón, CSIC-Universidad de Zaragoza, Plaza San Francisco s/n, 50009 Zaragoza, Spain

S Supporting Information

ABSTRACT: The terdentate anionic picolinate-based nitronyl nitroxide (picNN) free radical forms neutral and robust homoleptic complexes with rare earth-metal ions. The nonacoordinated Tb³⁺ complex Tb(picNN)₃·6H₂O is a single-molecule magnet with an activation energy barrier $\Delta = 22.8 \pm 0.5$ K and preexponential factor $\tau_0 = (5.5 \pm 1.1) \times 10^{-9}$ s. It shows magnetic hysteresis below 1 K.

The coordination chemistry of lanthanoid ions has been fueled by the potential applications of their optical and magnetic properties in bioassays and clinical diagnosis.^{1,2} In the field of molecular magnets, paramagnetic lanthanoid ions have been used as sources of large and anisotropic magnetic moments in the search of high coercivity. In this respect, the main disadvantage of these compounds is the internal character of their 4f unpaired electrons, which results in weak magnetic interactions between the spin carriers.^{3–7}

The report of Ishikawa and co-workers on lanthanoid double-decker complexes functioning as magnets at the single-molecular level produced a renaissance of lanthanoid chemistry in the context of molecular magnetic materials.⁸ Since then, several single-molecule magnets (SMMs) comprising lanthanoid ions, either isolated or interacting with other spin carriers, have been reported.⁹ Their high magnetic anisotropy provides an alternative to SMM based on polynuclear 3d systems with a high-spin ground state. To date, however, magnetic studies on SMM based on lanthanoid-radical systems are relatively scarce and are limited to dynamic properties.¹⁰ A few studies on mononuclear lanthanoid nitronyl nitroxide (NN) complexes have only recently been published.¹¹

Our interest lies in the coordination chemistry of a novel picolinate-based NN free radical that affords neutral complexes with 3d or 4f metal ions. Recently, we reported on the synthesis and magnetic behavior of the family of first-row transition-metal complexes [M(picNN)₂]·3H₂O featuring very strong metal-radical antiferromagnetic interactions.¹² In this article, the synthesis, structural characterization, and magnetic behavior (including static properties) of the novel mononuclear lanthanoid-radical complex [Tb(picNN)₃]·6H₂O (**1**) will be described.¹³

Compound **1** crystallizes in the monoclinic C2/c space group. The three picNN ligands (Figure 1) coordinate to the lanthanoid center in a terdentate binding mode, yielding a coordination

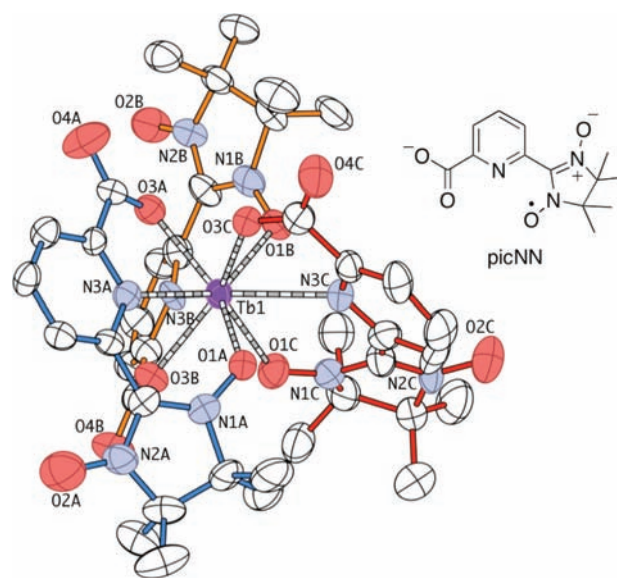


Figure 1. Thermal ellipsoid plot (50% probability) of **1**.

number of 9 for the Tb³⁺ ion. For nine-coordinated species, the idealized coordination geometries are tricapped trigonal prism (TTP) and capped square antiprism (CSAP).² Owing to the terdentate nature of the picNN ligand, the symmetry of the complex is best described assuming a distorted TTP structure, with six O atoms occupying the trigonal faces of the prism and three N(pyridine) atoms located in the capping positions. One of the trigonal faces is formed by coordination of two NN radicals and one carboxylate anion, while the second trigonal face contains the third NN radical and two carboxylate anions. The Tb–N(pyridine) distances (mean value: 2.62 ± 0.05 Å) are longer than the Tb–O(aminoxyl) (mean value: 2.376 ± 0.015 Å) and Tb–O(carboxylate) distances (mean value: 2.334 ± 0.024 Å), as was expected from the well-known oxophilicity of the lanthanoid ion. The crystal packing of **1** shows very short intermolecular contacts between the noncoordinated aminoxyl units [O2B–O2B = $3.486(5)$ Å; O2C–O2C = $3.1540(10)$ Å] that form alternating chains running along the *c* axis (Figure S1 in the Supporting Information). The remaining free N–O moiety is

Received: May 18, 2011

Published: July 13, 2011

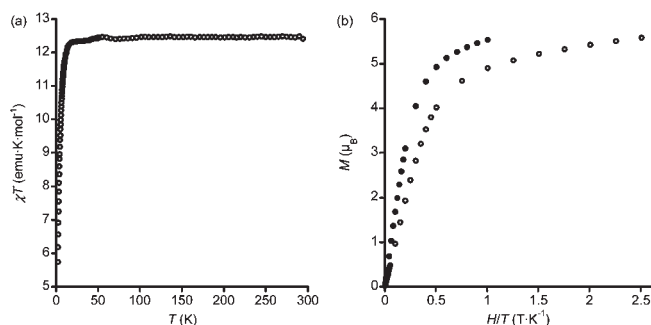


Figure 2. (a) Thermal variation of the χT product of **1**. (b) Reduced magnetization plots at 2 and 5 K.

hydrogen-bonded to a water molecule and isolated from the other radicals.

Temperature-dependent direct-current (dc) magnetic susceptibility data are displayed in Figure 2a as a $\chi T = f(T)$ plot. At room temperature, χT equals $12.4 \text{ emu} \cdot \text{K} \cdot \text{mol}^{-1}$, somewhat smaller than the sum of the expected paramagnetic contributions of one Tb^{3+} ion ($J = 6$, $11.81 \text{ emu} \cdot \text{K} \cdot \text{mol}^{-1}$) and three NN radicals ($S = 1/2$, $0.375 \text{ emu} \cdot \text{K} \cdot \text{mol}^{-1}$). The χT value remains constant with decreasing temperature to 15 K and then decreases abruptly to a value of $5.7 \text{ emu} \cdot \text{K} \cdot \text{mol}^{-1}$ at 2 K. This means that the combination of the splitting of the 7F_6 ground state due to crystal-field effects and the presence of intra- and intermolecular magnetic interactions¹⁴ between the free radicals overcomes the expected ferromagnetic terbium–radical interactions, leading to an effective antiferromagnetic behavior, as was previously observed in related compounds.^{10c}

The field dependences of magnetization at 2 and 5 K are shown in Figure 2b as M/μ_B versus H/T curves. In both cases, a sharp and linear increase of M takes place at low field. In the high-field region, the magnetization is far from the saturation value ($12 \mu_B$) expected for the four uncorrelated spins (one Tb^{3+} ion with $g \approx 3/2$ and $J = 6$ and three NN radicals with $g \approx 2$ and $S = 1/2$). Further, the curves at 2 and 5 K cannot be superimposed. These two facts point to the presence of a strong magnetic anisotropy in the system. No hysteresis effects are observed in this temperature range.

The dynamic magnetic properties of the material were investigated by alternating-current (ac) magnetic susceptibility (χ_{ac}) measurements in the 100–10 000 Hz frequency range under a zero static magnetic field. The thermal variation of the real (χ') and imaginary (χ'') components of χ_{ac} (Figure 3a,b) shows the presence of frequency-dependent signals at low temperatures. The χ' signal decreases as χ'' exhibits well-defined maxima at T_{\max} below 3 K. The temperature dependence of these peaks can be analyzed (Figure 3c) assuming a thermally activated process [Arrhenius law: $\tau = \tau_0 \exp(\Delta/kT)$], where $\tau = 1/2\pi\nu$, with ν being the frequency of the oscillating field. The resulting activation energy barrier $\Delta = 22.8 \pm 0.5 \text{ K}$ and preexponential factor $\tau_0 = (5.5 \pm 1.1) \times 10^{-9} \text{ s}$ compare well to those observed in other terbium(III) nitronyl nitroxide complexes displaying SMM character.¹¹ The maximal relative shift per decade of frequency [$\Delta T_{\max}/T_{\max} \Delta(\log \nu) = 0.22$] matches the value obtained for similar compounds, discarding a spin glass dynamics.

The frequency dependence of χ' and χ'' at different temperatures in the 2.2–4 K range was analyzed in the framework of the

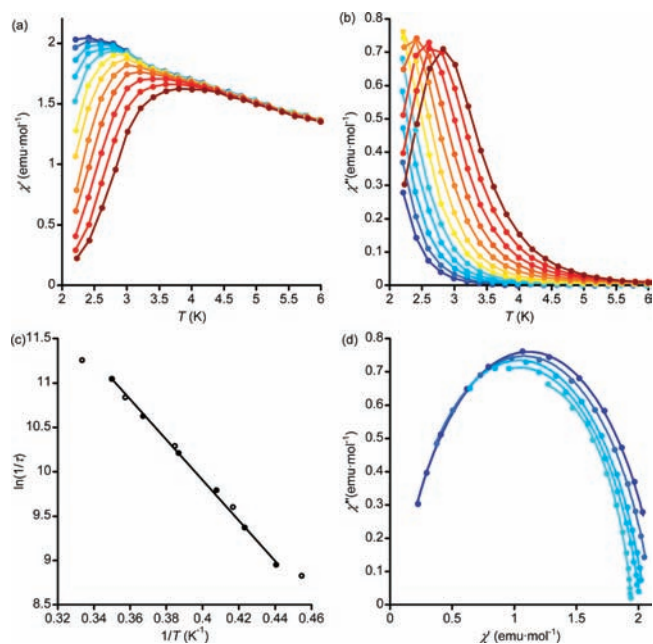


Figure 3. Thermal variation of χ' (a) and χ'' (b) of **1** for 10 logarithmically spaced frequencies between 100 Hz (blue) and 10 000 Hz (brown). (c) Arrhenius plot. Black circles are data obtained from the maxima of $\chi'' = f(T)$ curves; empty circles are best-fit data extracted from the Debye equation. (d) Argand plots at different temperatures. Lines refer to the best fit to the Cole–Cole equation.

Cole–Cole model, which accounts for a distribution of single relaxation processes:

$$\chi(\omega) = \chi_S + \frac{\chi_T - \chi_S}{1 + (i\omega\tau)^{1-\alpha}}$$

where χ_T and χ_S are respectively the isothermal and adiabatic susceptibilities, ω is the frequency of the ac field, τ is the relaxation time of the system, and α is a parameter indicating the width of the distribution. The extracted values of τ fitted the Arrhenius law exactly with the same parameters as mentioned above. Below 3 K, the distribution of relaxation times is relatively narrow and almost temperature-independent, with α values close to 0.2. This is best seen in the Argand plot (χ' and χ'' at a fixed temperature) shown in Figure 3d. At higher temperatures, α equals 0.1, indicating a narrower distribution. The system operates in a thermally activated regime (Figure 3c) in the whole temperature range, and its dynamic properties are strictly insensitive to the presence of a continuous magnetic field of 1000 Oe (Figure S2 in the Supporting Information). It seems then that the distribution of relaxation times appears from a distribution of local environments due to crystal defects.

According to the Arrhenius law, the relaxation time at the lowest temperature of the dc measurement (2 K) is very short ($\tau = 0.49 \text{ ms}$). This explains the absence of any hysteretic effect at this temperature. We thus investigated the magnetization of the sample at very low temperatures (0.35–3 K) using a micro-Hall probe. Below 1 K, an opening of the hysteresis loop is observed (Figure 4). The coercive field becomes independent of the temperature below 700 mK, suggesting that magnetization reverses via quantum tunnelling in this SMM. To our knowledge, this is the first evidence of hysteretic behavior in a lanthanoid–nitroxide complex.

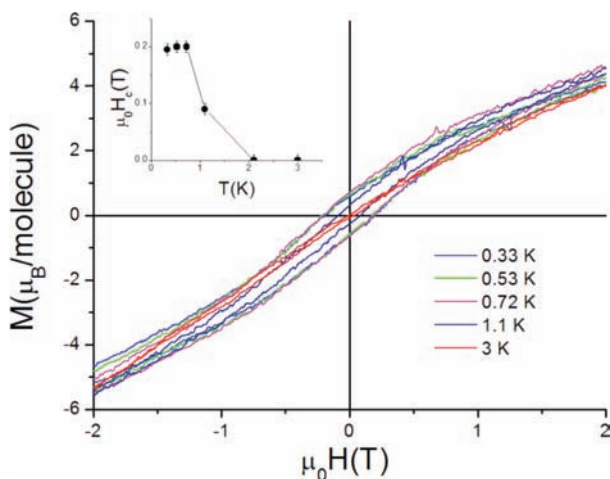


Figure 4. Magnetization hysteresis loops measured at the given temperatures. The magnetic field sweeping rate was $1 \text{ T} \cdot \text{min}^{-1}$. The inset shows the temperature dependence of the coercive magnetic field.

The reasons for the SMM behavior of terbium(III) complexes are well understood.⁸ The ligand field around the lanthanoid ion removes the 13-fold degeneracy of its $J = 6$ ground state. The lowest substates ($J_z = \pm 6$) are well separated from the rest of the energy levels, giving rise to a strong uniaxial anisotropy and a high energy barrier for reversal of the magnetic moments (from $J_z = +6$ to -6). The weak exchange coupling between the Tb^{3+} ion and the coordinated free radical does not alter the energy level scheme and the lanthanoid–radical complex retains its SMM characteristics. Also, antiferromagnetic radical–radical interactions are very important at the temperature range where the SMM properties are observed, preventing negative effects on the relaxation of the lanthanoid ion.

To summarize, we have used a terdentate NN anion to form a homoleptic neutral compound where the Tb^{3+} ion is coordinated to three radical units and retains its SMM behavior. For the first time, magnetic hysteresis loops have been recorded in a mononuclear lanthanoid–radical complex. Another novel aspect is the noncoordinated environment of Tb^{3+} , with previous studies on lanthanide–nitroxide complexes being restricted to 8- and 10-coordination. Preliminary studies show that these molecules can be deposited as self-assembled monolayers on metal surfaces as a first step in their potential use in spintronic applications.

ASSOCIATED CONTENT

Supporting Information. Crystallographic data (CIF format), a view of the crystal packing of **1** (Figure S1), ac magnetic properties in a continuous field of 1000 Oe (Figure S2), and magnetic properties of an isostructural yttrium(III) compound (Figure S3). This material is available free of charge via the Internet at <http://pubs.acs.org>.

AUTHOR INFORMATION

Corresponding Author

*E-mail: fmmr@uv.es.

ACKNOWLEDGMENT

We thank the European Union (NoE MagMaNet), Ministerio de Ciencia e Innovación (FEDER financed projects MAT2007-61584 MAT2009-13977-C03 and CONSOLIDER-

INGENIO 2010 CSD2007-00010), and Generalitat Valenciana (PROMETEO/2009/095).

REFERENCES

- (1) Parker, D. *Coord. Chem. Rev.* **2000**, *205*, 109.
- (2) Caravan, P.; Ellison, J. J.; McMurry, T. J.; Lauffer, R. B. *Chem. Rev.* **1999**, *99*, 2293–2352.
- (3) (a) Andruh, M.; Ramade, I.; Codjovi, E.; Guillou, O.; Kahn, O.; Trombe, J. C. *J. Am. Chem. Soc.* **1993**, *115*, 1822–1829. (b) Sanz, J. L.; Ruiz, R.; Gleiz, A.; Lloret, F.; Faus, J.; Julve, M.; Borrás-Almenar, J. J.; Journaux, Y. *Inorg. Chem.* **1996**, *35*, 7384–7393. (c) Costes, J.-P.; Dahan, F.; Dupuis, A.; Laurent, J.-P. *Chem.—Eur. J.* **1998**, *4*, 1616–1620. (d) Decurtins, S.; Gross, M.; Schmalke, H. W.; Ferlay, S. *Inorg. Chem.* **1998**, *37*, 2443. (e) Kahn, M. L.; Mathonière, C.; Kahn, O. *Inorg. Chem.* **1999**, *38*, 3692–3697. (f) Shiga, T.; Ohba, M.; Okawa, H. *Inorg. Chem.* **2004**, *43*, 4435–4446. (g) Andruh, M.; Costes, J.-P.; Diaz, C.; Gao, S. *Inorg. Chem.* **2009**, *48*, 3342–3359.
- (4) (a) Sutter, J.-P.; Kahn, M. L.; Golhen, S.; Ouahab, L.; Kahn, O. *Chem.—Eur. J.* **1998**, *4*, 571–576. (b) Kahn, M. L.; Sutter, J.-P.; Golhen, S.; Guionneau, P.; Ouahab, L.; Kahn, O.; Chasseau, D. *J. Am. Chem. Soc.* **2000**, *122*, 3413–3421.
- (5) (a) Lescop, C.; Belorizky, E.; Luneau, D.; Rey, P. *Inorg. Chem.* **2002**, *41*, 3375–3384. (b) Tsukuda, T.; Suzuki, T.; Kaizaki, S. *J. Chem. Soc., Dalton Trans.* **2002**, 1721–1726.
- (6) (a) Benelli, C.; Caneschi, A.; Gatteschi, D.; Sessoli, R. *Inorg. Chem.* **1993**, *32*, 4797–4801. (b) Benelli, C.; Caneschi, A.; Gatteschi, D.; Pardi, L.; Rey, P.; Shum, D. P.; Carlin, R. L. *Inorg. Chem.* **1989**, *28*, 272–275.
- (7) Norel, L.; Chamoreau, L. M.; Journaux, Y.; Oms, O.; Chastanet, G.; Train, C. *Chem. Commun.* **2009**, 2381–2383.
- (8) (a) Ishikawa, N.; Sugita, M.; Ishikawa, T.; Koshihara, S.; Kaizu, Y. *J. Am. Chem. Soc.* **2003**, *125*, 8694–8695. (b) Ishikawa, N.; Sugita, M.; Okubo, T.; Tanaka, N.; Iino, T.; Kaizu, Y. *Inorg. Chem.* **2003**, *42*, 2440–2446.
- (9) (a) Costes, J.-P.; Auchel, M.; Dahan, F.; Peyrou, V.; Shova, S.; Wernsdorfer, W. *Inorg. Chem.* **2006**, *45*, 1924–1934. (b) Mereacre, V.; Ako, A. M.; Clerac, R.; Wernsdorfer, W.; Hewitt, I. J.; Anson, C. E.; Powell, A. K. *Chem.—Eur. J.* **2008**, *14*, 3577–3584. (c) Aldamen, M. A.; Clemente-Juan, J. M.; Coronado, E.; Martí-Gastaldo, C.; Gaita-Ariño, A. *J. Am. Chem. Soc.* **2008**, *130*, 8874–8875. (d) Sessoli, R.; Powell, A. K. *Coord. Chem. Rev.* **2009**, *253*, 2328–2341.
- (10) (a) Poneti, G.; Bernot, K.; Bogani, L.; Caneschi, A.; Sessoli, R.; Wernsdorfer, W.; Gatteschi, D. *Chem. Commun.* **2007**, 1807–1809. (b) Tian, H.; Liu, R.; Wang, X.; Yang, P.; Li, Z.; Li, L.; Liao, D. *Eur. J. Inorg. Chem.* **2009**, 4498–4502. (c) Xu, J.-X.; Ma, Y.; Liao, D.; Xu, G.-F.; Tang, J.; Wang, C.; Zhou, N.; Yan, S.-P.; Cheng, P.; Li, L.-C. *Inorg. Chem.* **2009**, *48*, 8890–8896.
- (11) (a) Zhou, N.; Ma, Y.; Wang, C.; Xu, G. F.; Tang, J.-K.; Xu, J.-X.; Yan, S.-P.; Cheng, P.; Li, L.-C.; Liao, D.-Z. *Dalton Trans.* **2009**, 8489–8492. (b) Wang, X.-L.; Li, L.-C.; Liao, D.-Z. *Inorg. Chem.* **2010**, *49*, 4735–4737. (c) Bernot, K.; Pointillart, F.; Rosa, P.; Etienne, M.; Sessoli, R.; Gatteschi, D. *Chem. Commun.* **2010**, 6458–6460.
- (12) Coronado, E.; Giménez-Saiz, C.; Romero, F. M.; Tarazón, A. *Inorg. Chem.* **2009**, *48*, 2205–2214.
- (13) **Synthesis of $[\text{Tb}(\text{picNN})_3] \cdot 6\text{H}_2\text{O}$ (1).** A solution of radical picNN¹³ (100 mg, 0.35 mmol) in 3 mL of MeOH was added to a solution of $\text{Tb}(\text{NO}_3)_3 \cdot 6\text{H}_2\text{O}$ (40 mg, 0.088 mmol) in 3 mL of H_2O . The resulting blue solution was stirred for 24 h and then left undisturbed for 4 days. Slow evaporation of the solvent yielded blue-violet needles suitable for X-ray studies. Yield: 58 mg, 60%. ES-MS (CH_3OH): 991.27 $[\text{M} + \text{H}^+]^+$, 997.30 $[\text{M} + \text{Na}^+ - \text{O}]^+$, 1013.34 $[\text{M} + \text{Na}^+]^+$, 1029.19 $[\text{M} + \text{K}^+]^+$, 1036.36 $[\text{M} + 2\text{Na}^+ + \text{e}^-]^+$.
- (14) In order to seize the nature and strength of the intra- and intermolecular radical–radical interactions, we have synthesized an isostructural yttrium(III) compound. The study of the magnetic properties of pure and poly(ethylene glycol)-diluted samples of this complex reveals that both interactions are antiferromagnetic and that the intermolecular term dominates (Figure S3 in the Supporting Information).